International Journal of Solids and Structures 46 (2009) 2571–2576

Contents lists available at ScienceDirect

International Journal of Solids and Structures

journal homepage: www.elsevier.com/locate/ijsolstr

Propagation of bending waves in phononic crystal thin plates with a point defect

Zong-Jian Yao, Gui-Lan Yu *, Yue-Sheng Wang, Zhi-Fei Shi

School of Civil Engineering, Beijing Jiaotong University, Beijing 100044, PR China

ARTICLE INFO

Article history:
Received 22 October 2008
Received in revised form 17 January 2009
Available online 14 February 2009

Keywords:
Phononic crystal
Thin plate
Band gap
Bending waves
Defect states

ABSTRACT

In this paper, the band structures of bending waves in a phononic crystal thin plate with a point defect are studied using an improved plane wave expansion method combined with the supercell technique. In particular, a phononic crystal thin plate composed of an array of circular crystalline Al_2O_3 cylinders embedded in an epoxy matrix with a square lattice is considered in detail. Full band gaps are shown. When a point defect is introduced, the bending waves are highly localized at or near the defect, resulting in defect modes. The frequency and number of the defect modes are strongly dependent on the filling fraction of the system and the size of the point defect. The defect bands appear from the upper edge of the gap and move to the middle of the gap as the defect size is reduced. For a given defect, the frequencies of the defect bands increase as the filling fraction increases.

1. Introduction

Much attention has recently been paid to the propagation of elastic waves in acoustic band gap materials, called phononic crystals, which are made of two or more elastic materials with large contrast between their mechanical properties (elastic stiffness and/or mass density). The existence of complete phononic band gaps, or ranges of frequencies in which elastic waves are forbidden to propagate in any direction, suggests the possible application of phononic crystals as noise suppressors, perfect acoustic mirrors (Bria and Djafari-Rouhani, 2002), acoustic filters (Sigalas, 1998), etc. The band gap characteristics of the perfect bulk phononic crystals have been investigated extensively both theoretically and experimentally. Some numerical methods to calculate the band structures have been developed, including the plane wave expansion (PWE) method (Tanaka and Tamura, 1998; Wu et al., 2004), the multiple scattering theory (MST) (Psarobas et al., 2000), the finite difference time domain (FDTD) method (Garcia-Pablos et al., 2000), the wavelet method (Yan and Wang, 2006, 2007; Yan et al., 2008), and others. These numerical methods, combined with the supercell technique (Sigalas, 1997), have also been used to calculate the band structures of imperfect bulk phononic crystals with point or linear defects (see, e.g. Khelif et al., 2003; Kafesaki et al., 2001; Sigalas, 1998). The existence of defects may result in a high localization of elastic waves near the defects, making it possible to design novel microcavities (Khelif et al., 2003), high efficiency waveguides (Khelif et al., 2004; Torres et al., 1999), and frequency demultipliers (Benchabane et al., 2005) and couplers (Sun and Wu, 2005).

A few investigations have also been carried out for phononic crystals with finite thickness, i.e. phononic crystal plates. Among these studies, most are concerned with Lamb waves based on the three dimensional governing equations of elastic waves; for example, Charles et al. (2006) calculated the band structures for two different kinds of two-dimensional phononic guides using the PWE method, Sun and Wu (2007) studied the propagation of Lamb waves in a phononic crystal plate using the FDTD method, including the guided wave modes due to the linear defect, and Vasseur et al. (2007) examined the waveguides in a piezoelectric phononic crystal plate both freestanding and deposited on a silicon substrate with the help of the finite element method. Very recently, Vasseur et al. (2008) introduced a supercell PWE method to calculate the elastic band structures for Lamb waves in a special phononic crystal plate sandwiched between two slabs made of elastic homogeneous materials. Pennec et al. (2008) employed both the FDTD method and the finite element method to investigate the dispersion of Lamb waves in a structure consisting of cylindrical dots deposited on a thin homogeneous plate. The linear defect modes were also studied. It was found that this structure can exhibit a low frequency gap.

It is known that the bending wave modes are dominant when the plate is relatively thin, and thus plate theory is generally used in this case. Sigalas and Economou (1994) calculated the dispersion relations of bending waves propagating in thin plates using the PWE method. Yu et al. (2006) investigated the band structures of a thin plate with 2D binary locally resonant structures using the improved PWE method (Li, 1996; Cao et al., 2004). Hsu and Wu (2006) studied the propagation of waves in a phononic crystal plate based on the Mindlin plate theory. Until now, however, no studies have been devoted to bending waves in a plate with

* Corresponding author. Tel.: +86 10 51688277; fax: +86 10 51687248.
E-mail address: glyu@bjtu.edu.cn (G.-L. Yu).

0020-7683/$ - see front matter © 2009 Elsevier Ltd. All rights reserved.
doi:10.1016/j.ijsolstr.2009.02.002

defects. In this paper, the band structures of phononic crystal thin plates with a point defect are investigated based on the classical plate theory using the improved PWE method combined with the supercell technique.

2. Theory

Fig. 1 shows a phononic crystal thin plate. The system is composed of an infinite periodic array of circular cylinders (material A) embedded periodically in a host matrix (material B). Both elastic materials A and B are isotropic. The thickness of the thin plate, the lattice constant and the radius of the cylinder are denoted by h, a and r_0, respectively.

In terms of the (x,y,z)-coordinate system, where the x- and y-axes are in the plane of the plate as shown in Fig. 1, the equation governing the bending of a plate with uniform thickness is (Sigalas and Economou, 1994)

$$-\alpha\frac{\partial^2 w}{\partial t^2}=\frac{\partial^2}{\partial x^2}\left(D\frac{\partial^2 w}{\partial x^2}+\beta\frac{\partial^2 w}{\partial y^2}\right)+2\frac{\partial^2}{\partial x\partial y}\left(\gamma\frac{\partial^2 w}{\partial x\partial y}\right)+\frac{\partial^2}{\partial y^2}\left(D\frac{\partial^2 w}{\partial y^2}+\beta\frac{\partial^2 w}{\partial x^2}\right), \tag{1}$$

where w is the transverse displacement in the z-direction, $D = Eh^3/12(1-\nu^2)$ is the flexural rigidity with E being the Young's modulus and ν the Poisson's ratio, $\alpha = \rho h$, $\beta = D\nu$ and $\gamma = D(1-\nu)$. All of these quantities are periodic functions of the position vector $\mathbf{r} = (x,y)$.

A generally used method to solve the above equation is the conventional PWE method. However, the slow convergence of the method is always a problem, especially for systems with a large elastic mismatch. Cao et al. (2004) proposed a new formulation of the PWE method for band structure calculation and showed that the new formulation can provide much more accurate numerical results than the conventional PWE method, especially for systems with a large elastic mismatch. In the present paper, the new formulation is adopted to expedite convergence and is referred to as the improved PWE method. For details about this new formulation, we refer the reader to Li (1996) and Cao et al. (2004).

According to Bloch's theorem, the displacement fields of harmonic waves in the phononic crystal thin plate can be expressed as

$$w(\mathbf{r},t)=\mathrm{e}^{i(\mathbf{k}\cdot\mathbf{r}-\omega t)}w_k(\mathbf{r}), \tag{2}$$

where $\mathbf{k} = (k_1,k_2)$ is the Bloch wave vector and ω is the angular frequency. $w_k(\mathbf{r})$ is a periodic function with the same spatial periodicity as the structure and can be expanded in Fourier series as

$$w_k(\mathbf{r})=\sum_{G_1}\mathrm{e}^{i\mathbf{G}_1\cdot\mathbf{r}}A_{\mathbf{G}_1}, \tag{3}$$

where $\mathbf{G}_1 = 2\pi(n_1/a, n_2/a)$ is the 2D reciprocal lattice vector with n_1, $n_2 = 0, \pm1, \pm2, \ldots \pm n$ and $A_{\mathbf{G}_1}$ is the corresponding Fourier coefficient.

In the conventional PWE method, the material parameters are all directly expanded in Fourier series according to the spatial periodicity. In the improved PWE method, however, the inverses of the material parameters (excluding the mass density) are expanded in Fourier series in order to get a good convergence (Li, 1996; Cao et al., 2004). For the present problem, we expand $\alpha(\mathbf{r})$, $1/\beta(\mathbf{r})$, $1/D(\mathbf{r})$ and $1/\gamma(\mathbf{r})$ in a Fourier series of the following form:

$$H(\mathbf{r})=\sum_{\mathbf{G}_2}e^{i\mathbf{G}_2\cdot\mathbf{r}}H_{\mathbf{G}_2} \tag{4}$$

with

$$H_{\mathbf{G}_2}=\begin{cases} fH_A+(1-f)H_B & \text{for}\quad \mathbf{G}_2=0 \\ (H_A-H_B)F_{G_2} & \text{for}\quad \mathbf{G}_2\neq 0 \end{cases}, \tag{5}$$

where $H(\mathbf{r})$ can be one of $\alpha(\mathbf{r})$, $1/\beta(\mathbf{r})$, $1/D(\mathbf{r})$ or $1/\gamma(\mathbf{r})$, $H_{\mathbf{G}_2}$ is the corresponding Fourier coefficient, $\mathbf{G}_2 = 2\pi(n_1/a, n_2/a)$, $n_1, n_2 = 0, \pm1, \pm2, \ldots \pm n$, and f is the filling fraction of each inclusion, defined as the ratio between the cross sectional area of a cylinder and that of the primitive unit cell. $F_{\mathbf{G}_2}$ is the structure function, defined as

$$F_{G_2}=\frac{1}{S}\int_A e^{-i\mathbf{G}\cdot\mathbf{r}}\mathrm{d}r^2,$$

with S denoting the area of the unit cell and the integral being performed over the cross section of the material A. For circular cylinders with radius r_0, $f=\pi r_0^2/a^2$ and $F_{\mathbf{G}_2}=2fJ_1(|\mathbf{G}_2|r_0)/|\mathbf{G}_2|r_0$ with $J_1(|\mathbf{G}_2|r_0)$ being the first order Bessel function of the first kind.

Considering Eqs. (1)–(5), we have the following eigenvalue problem:

$$\begin{aligned}\omega^2\sum_{\mathbf{G}_1}[\![\alpha]\!]_{\mathbf{G}_2}\mathbf{A}_{\mathbf{k}+\mathbf{G}_1} = {} & \sum_{\mathbf{G}_1}(\mathbf{k}+\mathbf{G}_1)_x^2(\mathbf{k}+\mathbf{G}_3)_x^2[\![1/\mathbf{D}]\!]_{\mathbf{G}_2}^{-1}\mathbf{A}_{\mathbf{k}+\mathbf{G}_1} \\ & +\sum_{\mathbf{G}_1}(\mathbf{k}+\mathbf{G}_1)_y^2(\mathbf{k}+\mathbf{G}_3)_x^2[\![1/\beta]\!]_{\mathbf{G}_2}^{-1}\mathbf{A}_{\mathbf{k}+\mathbf{G}_1} \\ & +2\sum_{\mathbf{G}_1}(\mathbf{k}+\mathbf{G}_1)_x(\mathbf{k}+\mathbf{G}_1)_y(\mathbf{k}+\mathbf{G}_3)_x \\ & \times(\mathbf{k}+\mathbf{G}_3)_y[\![1/\gamma]\!]_{\mathbf{G}_2}^{-1}\mathbf{A}_{\mathbf{k}+\mathbf{G}_1}+\sum_{\mathbf{G}_1}(\mathbf{k}+\mathbf{G}_1)_y^2 \\ & \times(\mathbf{k}+\mathbf{G}_3)_y^2[\![1/\mathbf{D}]\!]_{\mathbf{G}_2}^{-1}\mathbf{A}_{\mathbf{k}+\mathbf{G}_1}+\sum_{\mathbf{G}_1}(\mathbf{k}+\mathbf{G}_1)_x^2 \\ & \times(\mathbf{k}+\mathbf{G}_3)_y^2[\![1/\boldsymbol{\beta}]\!]_{\mathbf{G}_2}^{-1}\mathbf{A}_{\mathbf{k}+\mathbf{G}_1},\end{aligned} \tag{6}$$

where $\mathbf{G}_3 = \mathbf{G}_1 + \mathbf{G}_2$ and $[\![\mathbf{H}]\!]_{\mathbf{G}_2}^{-1}$ denotes the inverse of the Toeplitz matrix $[\![\mathbf{H}]\!]_{\mathbf{G}_2}$ with elements shown in Eq. (5) (Li, 1996; Cao et al., 2004). Truncating the series in Eq. (6) to finite sums consisting of N terms, we can obtain $N \times N$ equations, and Eq. (6) can then be rewritten in matrix form:

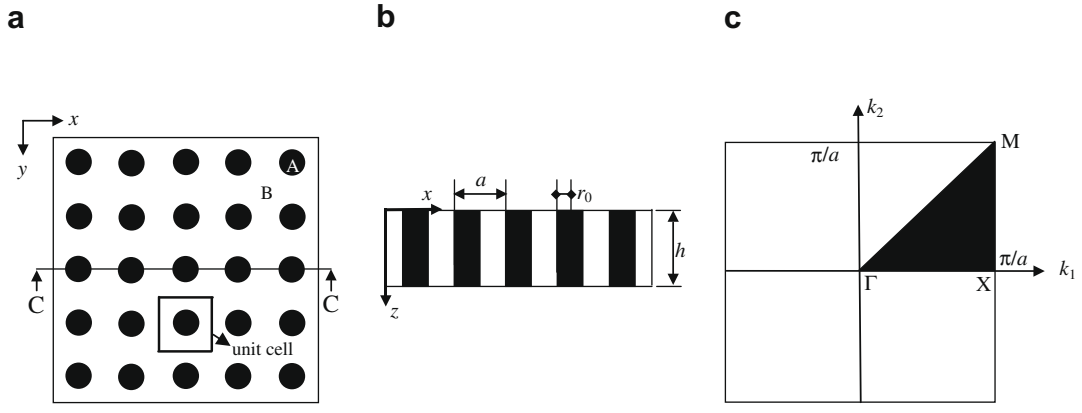

Fig. 1. An infinite phononic crystal thin plate: (a) the square lattice, (b) the cross section cutting along the line C–C in (a), and (c) the corresponding first Brillouin zone.

$$\omega^2 \mathbf{P}\mathbf{A}_{\mathbf{k}+\mathbf{G}_1} = \mathbf{Q}\mathbf{A}_{\mathbf{k}+\mathbf{G}_1}, \tag{7}$$

where $\mathbf{P}$ and $\mathbf{Q}$ are $N \times N$ matrixes,

$$\mathbf{P} = \sum_{\mathbf{G}_1} [\![\alpha]\!]_{\mathbf{G}_2}, \tag{8}$$

$$\begin{aligned}\mathbf{Q} = & \sum_{\mathbf{G}_1} (\mathbf{k}+\mathbf{G}_1)_x^2 (\mathbf{k}+\mathbf{G}_3)_x^2 [\![1/\mathbf{D}]\!]_{\mathbf{G}_2}^{-1} + \sum_{\mathbf{G}_1} (\mathbf{k}+\mathbf{G}_1)_y^2 \\ & \times (\mathbf{k}+\mathbf{G}_3)_x^2 [\![1/\beta]\!]_{\mathbf{G}_2}^{-1} + 2\sum_{\mathbf{G}_1} (\mathbf{k}+\mathbf{G}_1)_x (\mathbf{k}+\mathbf{G}_1)_y (\mathbf{k}+\mathbf{G}_3)_x \\ & \times (\mathbf{k}+\mathbf{G}_3)_y [\![1/\gamma]\!]_{\mathbf{G}_2}^{-1} + \sum_{\mathbf{G}_1} (\mathbf{k}+\mathbf{G}_1)_y^2 (\mathbf{k}+\mathbf{G}_3)_y^2 [\![1/\mathbf{D}]\!]_{\mathbf{G}_2}^{-1} \\ & + \sum_{\mathbf{G}_1} (\mathbf{k}+\mathbf{G}_1)_x^2 (\mathbf{k}+\mathbf{G}_3)_y^2 [\![1/\beta]\!]_{\mathbf{G}_2}^{-1}. \end{aligned} \tag{9}$$

The eigenfrequency ω can be obtained by solving Eq. (7) for a specific Bloch vector k, yielding the band structures.

It should be noted that the classical plate theory used in this paper is applicable only for a thin plate and long wavelengths, so that $kh \ll 1$, $h/a \ll 1$. Mindlin's plate theory could avoid this limitation, but it is more complex mathematically (Hsu and Wu, 2006). Here, as a preliminary investigation of the defect state of the bending wave modes, we use the classical plate theory.

3. Band structures for a perfect phononic crystal thin plate

We consider bending waves propagating in a perfect phononic crystal thin plate with cylindrical inclusions of Al_2O_3 (material A) embedded periodically in the Epoxy host (material B) as shown in Fig. 1a. The mechanical properties used in the following calculations are $\rho_A = 3970\ kg/m^3$, $E_A = 402.7$ GPa, and $\nu_A = 0.23$, and $\rho_B = 1142\ kg/m^3$, $E_B = 4.35$ GPa, and $\nu_B = 0.378$. The thickness of the plate is h=0.1a, and the transverse wave velocity in Epoxy is $C_t = 1160$ m/s.

Fig. 2 displays the band structure along the closed path $M-\Gamma-X-M$ in the first irreducible Brillouin zone shown in Fig. 1c with filling fraction $f = 0.283$. The frequency is normalized by a/C_t. We find that there exist two complete band gaps. The first one, which is much wider than the second one, is located in the normalized frequency region $3.37 \sim 4.63$.

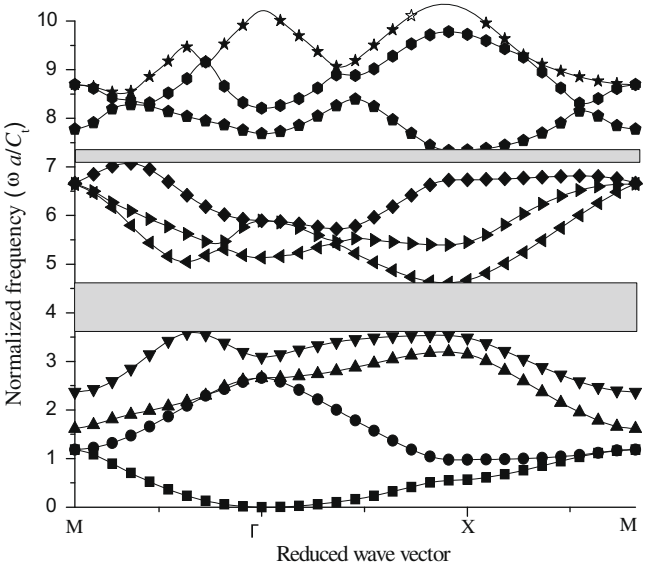

Fig. 2. Band structures of the perfect phononic crystal thin plate (Al_2O_3/Epoxy) of a square lattice with $f = 0.283$.

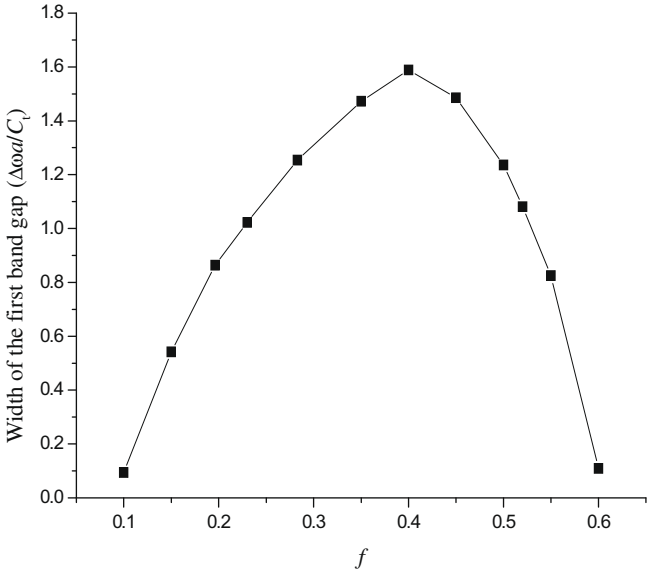

Fig. 3. The normalized first band gap width varying with the filling fraction.

The width of the first band gap as a function of the filling fraction is shown in Fig. 3. We can see that the band gap exists for filling fractions varying from 0.1 to 0.6. With the filling fraction increasing, the width of the band gap increases to a maximum and then decreases. Fig. 3 shows that the optimal filling fraction giving a maximum gap width for the Al_2O_3/Epoxy thin plate is $f = 0.4$.

4. Band structures for a phononic crystal thin plate with a point defect

Now we examine the band structures of the thin plate when a point defect is introduced. The defect is created by changing the radius of one of the cylinders. The theoretical analysis of the defect modes can be carried out by the supercell technique that has been performed successfully for the study of defect states in 2D bulk phononic crystals (Sigalas, 1998; Wu et al., 2001; Yan et al., 2008). The basic idea of the supercell technique is to select an $M \times M$ supercell including the defect and impose Born-von-Karmon periodic conditions on the boundary of the supercell (Sigalas, 1998; Yan et al., 2008). Previous calculations have shown that a 5×5 supercell can yield accurate results (Sigalas, 1998; Wu et al., 2001; Yan et al., 2008). Therefore, in our computation we choose a 5×5 supercell containing the point defect as shown in Fig. 4a, where the hollow circle indicates the point defect with radius r_d. The corresponding irreducible part of the first Brillouin zone is shown in Fig. 4b. The Fourier coefficient $H_{\mathbf{G}}$ in Eq. (4) is now changed to

$$H_{\mathbf{G}} = \begin{cases} \frac{1}{25}\{24[fH_A + (1-f)H_B] + f_d H_A + (1-f_d)H_B\} & \text{for } G = 0 \\ \frac{1}{25}(H_A - H_B)\left\{\left[\sum_{m_1=-2}^{2}\sum_{m_2=-2}^{2} \cos\left(\frac{2\pi}{5}(m_1 n_1 + m_2 n_2)\right) - 1\right] F_{\mathbf{G}} + F_{\mathbf{G}}^{d}\right\} & \text{for } \mathbf{G} \neq 0 \end{cases}, \tag{10}$$

where $\mathbf{G} = 2\pi(n_1/5a, n_2/5a)$ is the reciprocal lattice vector with n_1, $n_2 = 0, \pm1, \pm2, \ldots n$ and $F_{\mathbf{G}}^{d} = 2f_d J_1(|\mathbf{G}|r_0)/|\mathbf{G}|r_0$ is the structure function of the defect cylinder with $f_d = \pi r_d^2/a^2$ being the defect filling ratio.

Following the same process as the one used in the perfect plate calculation, the band structures of bending waves in the thin plate with different values of defect cylinder radius r_d are shown in Fig. 5. In all, 1089 plane waves are employed, and the calculating accuracy can be seen from Table 1, which displays the frequencies

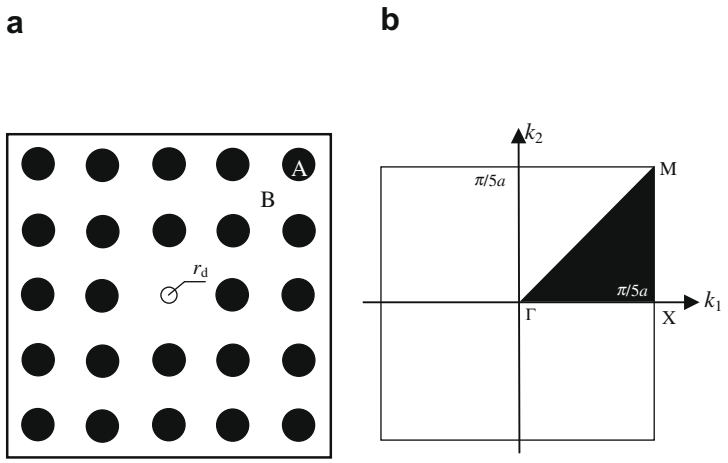

Fig. 4. (a) The 5 × 5 supercell, and (b) the corresponding first Brillouin zone.

varying with the number of plane waves for the points A, B, and C marked in Fig. 5. The filling fraction of the corresponding perfect system is $f = 0.283$. It can be seen from Fig. 5 that the flat defect bands, which are nondegenerate, start to appear from the upper edge of the gap and finally fall in the middle. Similar behaviors have been found in 2D infinite systems (Sigalas, 1997).

Fig. 6 shows in detail how the frequencies of defect modes change with defect radius for the given filling fraction $f = 0.283$. More defect bands (up to three) appear inside the first band gap as the radius ratio r_d/r_0 decreases from 0.8 to 0. All defect bands move from the upper edge towards the middle as r_d decreases. The edges of the first band gap remain almost unchanged as r_d varies.

The displacement distributions associated with the three defect modes with $r_d/r_0 = 0.2$ at the Γ point in the 5 × 5 supercell are shown in Fig. 7. The cylinders are located at $[(2n_x + 1)/2,(2n_y + 1)/2]$, $(n_x, n_y = 0, 1, 2, 3, 4)$ and the defect cylinder is at the center. The results show their peculiar symmetry. It can be clearly seen that for the two lower defect modes, the displacement amplitudes around the defect are much bigger than those at or far away from the defect (see Fig. 7a and b). However, for the higher defect mode, the displacement amplitude reaches a maximum at the defect cylinder and decays rapidly with distance away from the defect (see Fig. 7c). Obviously, the bending waves corresponding to the three modes are so localized at or near the defect that they cannot escape into the surrounding media. In other words, the point defect behaves like a vacant resonator. It can be also seen that the degree

Table 1
Variation of the normalized frequencies with the number of plane waves $(2n + 1)^2$ employed in the calculation for points A, B, and C marked in Fig. 5.

n	ω_1	ω_2	ω_3
8	2.8553	3.4175	3.5078
9	3.0758	3.4931	3.5988
10	3.1144	3.6773	4.1838
11	3.1451	3.7556	4.3722
12	3.1694	3.7971	4.3871
13	3.2196	3.8247	4.4139
14	3.2319	3.8405	4.4174
15	3.2963	3.8870	4.4880
16	3.2983	3.9209	4.5002
17	3.3085	3.9427	4.5322

ω_1 – the frequency of the lower edge of the band gap marked by A; ω_2 – the frequency of the defect band marked by B; ω_3 – the frequency of the upper edge of the band gap marked by C.

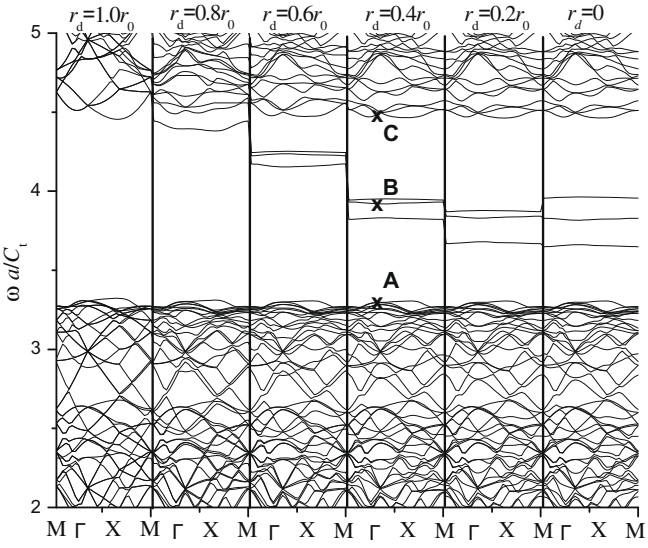

Fig. 5. Band structures of the phononic crystal thin plate (Al_2O_3/Epoxy) with a point defect for $f = 0.283$.

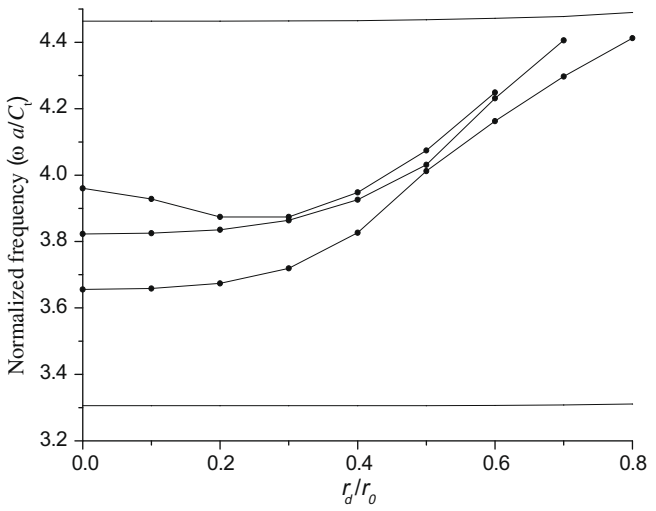

Fig. 6. Frequencies of the defect modes versus radius ratio r_d/r_0 at filling fraction $f = 0.283$ in the Al_2O_3/Epoxy system.

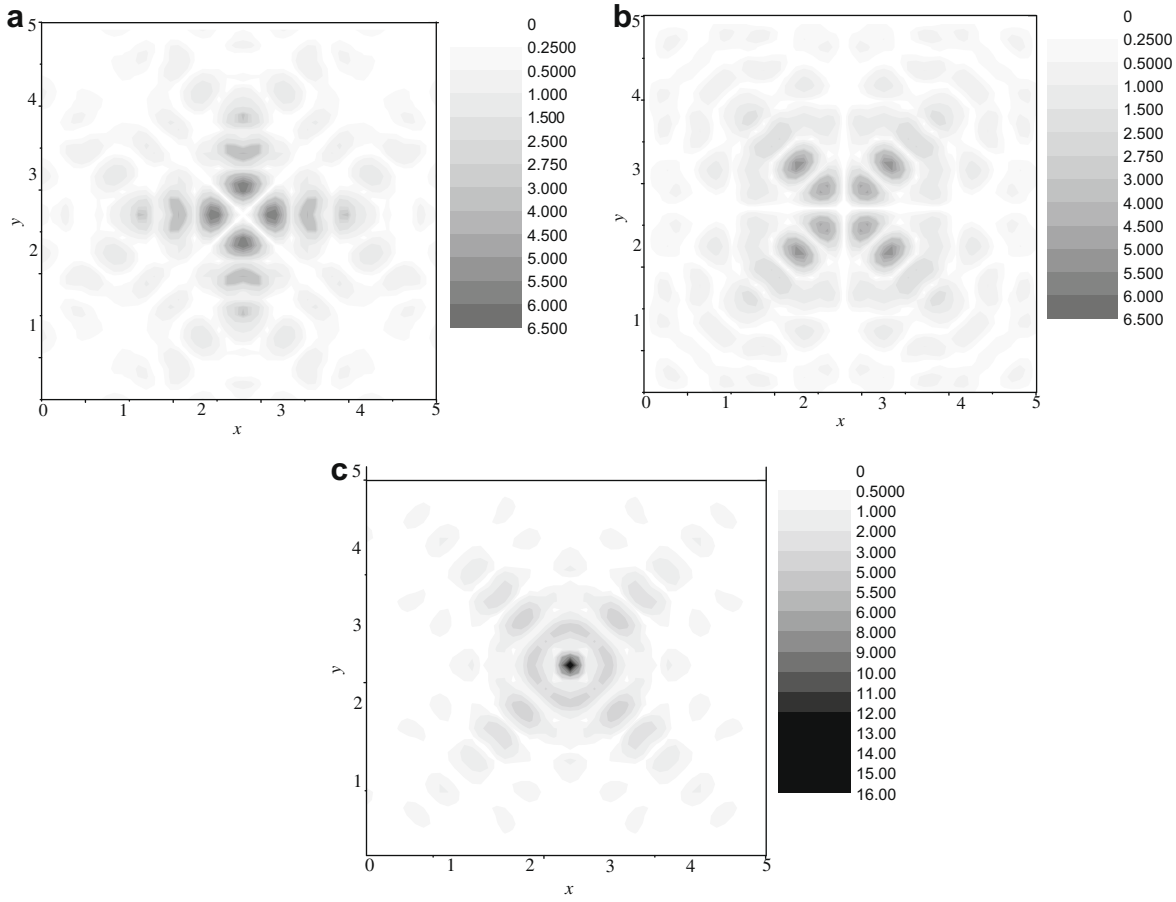

Fig. 7. The displacement distribution in the 5 × 5 supercell with r_d/r_0=0.2 at the Γ point corresponding to the three defect modes (a) $\omega a/C_t$ = 3.680, (b) $\omega a/C_t$ = 3.829, and (c) $\omega a/C_t$ = 3.878.

of localization for the third defect mode (shown in Fig. 7c) is much higher than for the other two.

Fig. 8 shows the frequencies of the defect modes as a function of filling fraction for r_d = 0. The lines with dots indicate the frequencies of the defect modes, and the solid lines show the edges of the first band gap. We can see that the frequencies of the defect modes increase as the filling fraction increases. There are up to five nondegenerate defect bands emerging from inside the first band gap. The number of defect bands increases from 1 to 5 as the filling fraction increases from 0.11 to 0.5, before decreasing to 1 as the filling fraction increases to 0.55. The defect bands disappear at very low and very high filling fractions.

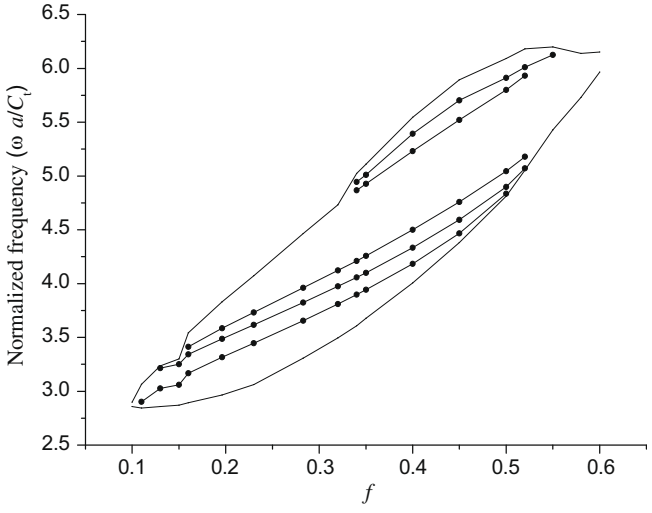

Fig. 8. Defect modes versus filling fraction for r_d = 0.

5. Conclusions

Based on the improved PWE method combined with the supercell technique, the band structures of bending waves in the phononic crystal thin plate of Al_2O_3/Epoxy with a point defect have been calculated. The defect modes existing in the first band gap are shown to be strongly dependent on the size of the point defect and the filling fraction of the system. For a given filling fraction, the defect bands appear from the upper edge of the gap and move to the middle of the gap as the defect size is reduced. For a given defect, the number of the defect bands varies between 0 and 5 in a certain range of the filling fraction, and the frequencies of the defect bands increase with increasing filling fraction. The displacement distributions show that the bending waves are highly localized at or near the defect, and the degrees of localization are different for different modes. This study provides a foundation in theory to design acoustic filters in engineering applications.

Acknowledgement

The work is supported by China National Science Foundation under Grant Nos. 10632020 and 90715006.

References

Benchabane, S., Khelif, A., Choujaa, A., Djafari-Rouhani, B., Laude, V., 2005. Interactioin of waveguide and localized modes in a phononic crystal. Europhysics Letters 71 (4), 570–575.

Bria, D., Djafari-Rouhani, B., 2002. Omnidirectional elastic band gap in finite lamellar structures. Physical Review E 66, 056609.

Cao, Y.J., Hou, Z.L., Liu, Y.Y., 2004. Convergence problem of plane-wave expansion method for phononic crystals. Physics Letters A 327, 247–253.

Charles, C., Bonello, B., Ganot, F., 2006. Propagation of guided elastic waves in 2D phononic crystals. Ultrasonics 44, e1209–e1213.

Garcia-Pablos, D., Sigalas, M., Montero de Espinosa, F.R., Torres, M., Kafesaki, M., Garcia, N., 2000. Theory and experiments on elastic band gaps. Physical Review Letters 84, 4349–4352.

Hsu, J.C., Wu, T.T., 2006. Efficient formulation for band-structure calculations of two-dimensional phononic-crystal plates. Physical Review B 74, 144303.

Khelif, A., Choujaa, A., Benchabane, S., Djafari-Rouhani, B., Laude, V., 2004. Guiding and bending of acoustic waves in highly confined phononic crystal waveguides. Applied Physics Letters 84 (22), 4400–4402.

Khelif, A., Choujaa, A., Djafari-Rouhani, B., Wilm, M., Ballandras, S., Laude, V., 2003. Trapping and guiding of acoustic waves by defect modes in a full-band-gap ultrasonic crystal. Physical Review B 68, 214301.

Kafesaki, M., Sigalas, M.M., Garcia, N., 2001. Wave guides in two-dimensional elastic wave band-gap materials. Physica B 296, 190–194.

Li, L.F., 1996. Use of Fourier series in the analysis of discontinuous periodic structures. Journal of the Optical Society of America 13, 1870–1876.

Pennec, Y., Djafari-Rouhani, B., Larabi, H., Vasseur, J.O., Hladky-Hennion, A.-C., 2008. Low-frequency gaps in a phononic crystal constituted of cylindrical dots deposited on a thin homogeneous plate. Physical Review B 78, 104105.

Psarobas, I.E., Stefanou, N., Modinos, A., 2000. Scattering of elastic waves by periodic arrays of spherical bodies. Physical Review B 62, 278–291.

Sigalas, M.M., 1997. Elastic wave band gaps and defect states in two-dimensional composites. Journal of the Acoustical Society of America 101, 1256–1261.

Sigalas, M.M., 1998. Defect states of acoustic waves in a two-dimensional lattice of solid cylinders. Journal of Applied Physics 84, 3026–3030.

Sigalas, M.M., Economou, E.N., 1994. Elastic waves in plates with periodically placed inclusions. Journal of Applied Physics 75, 2845–2850.

Sun, J.H., Wu, T.T., 2005. Analyses of mode coupling in joined parallel phononic crystal waveguides. Physical Review B 71, 174303.

Sun, J.H., Wu, T.T., 2007. Propagation of acoustic waves in phononic-crystal plates and waveguides using a finite-difference time-domain method. Physical Review B 76, 104304.

Torres, M., Montero de Espinosa, F.R., Garcia-Pablos, D., Garcia, N., 1999. Sonic band gaps in finite elastic media: surface states and localization phenomena in linear and point defects. Physical Review Letters 82, 3054–3057.

Tanaka, Y., Tamura, S.I., 1998. Surface acoustic waves in two-dimensional periodic elastic structures. Physical Review B 58, 7958–7965.

Vasseur, J.O., Deymier, P.A., Djafari-Rouhani, B., Pennec, Y., Hladky-Hennion, A.-C., 2008. Absolute forbidden bands and waveguiding in two-dimensional phononic crystal plates. Physical Review B 77, 085415.

Vasseur, J.O., Hladky-Hennion, A.-C., Djafari-Rouhani, B., Duval, F., Dubus, B., Pennec, Y., Deymier, P.A., 2007. Waveguiding in two-dimensional piezoelectric phononic crystal plates. Journal of Applied Physics 101, 114904.

Wu, F.G., Hou, Z.L., Liu, Z.Y., Liu, Y.Y., 2001. Point defect states in two-dimensional phononic crystals. Physics Letters A 292, 198–202.

Wu, T.T., Huang, Z.G., Lin, S., 2004. Surface and bulk acoustic waves in two-dimensional phononic crystal consisting of materials with general anisotropy. Physical Review B 69, 094301.

Yan, Z.Z., Wang, Y.S., 2006. Wavelet-based method for calculating elastic band gaps of two-dimensional phononic crystals. Physical Review B 74 (22), 224303.

Yan, Z.Z., Wang, Y.S., 2007. Wavelet-based method for computing elastic band gaps of one-dimensional phononic crystals. Science in China Series G: Physics Mechanics and Astronomy 50 (5), 622–630.

Yan, Z.Z., Wang, Y.S., Zhang, Ch., 2008. Wavelet method for calculating the defect states of two-dimensional phononic crystals. Acta Mechanica Solida Sinaca 21, 104–109.

Yu, D.L., Wang, G., Liu, Y.Z., Wen, J.H., Qiu, J., 2006. Flexural vibration band gaps in thin plates with two-dimensional binary locally resonant structures. Chinese Physics 15, 266–271.